

Origin of ^3He abundance enhancements in gradual solar energetic particle events

Radoslav Bučik¹, Samuel T. Hart^{2,1}, Maher A. Dayeh^{1,2}, Mihir I. Desai^{1,2}, Glenn M. Mason³ and Mark E. Wiedenbeck⁴

¹Southwest Research Institute, San Antonio, TX, USA

²University of Texas at San Antonio, San Antonio, TX, USA

³Johns Hopkins University, Applied Physics Laboratory, Laurel, MD, USA

⁴Jet Propulsion Laboratory, California Institute of Technology, Pasadena, CA, USA

Abstract. We examined the origin of ^3He abundance enhancement in 23 high-energy (25–50 MeV) solar proton events that coincide with ^3He -rich periods detected by ACE ULEIS in 1997–2021. In seven events, ^3He enhancement was due to ^3He leftover from preceding events or independent ^3He events occurring during proton events. One event is the most likely impulsive (^3He -rich), and another is unclear. Reaccelerated remnant flare material was the most probable cause of ^3He enhancements in the remaining 14 proton events. Imaging observations showed coronal jets in the parent active regions in six of these 14 events. Remarkably, the highest $^3\text{He}/^4\text{He}$ occurred in events with jets, implying their contribution to ^3He enhancement.

Keywords. Elemental composition, Particle acceleration, CME

1. Introduction

Coronal mass ejection (CME)-shock-related (or gradual) solar energetic particle (SEP) events show extensive event-to-event compositional variations whose origin is largely unexplored. The events often exhibit high abundance enhancement of ^3He and heavy ions, typical of flare-related (or impulsive) SEP events. Mason et al. (1999) examined 12 gradual SEP (GSEP) events and found in eight events the 0.5–2.0 MeV/nuc $^3\text{He}/^4\text{He}$ between 5 and 135 times the average slow solar wind (SSW) ratio (Gloeckler and Geiss 1998). Desai et al. (2016) found in 27 out of 46 GSEP events the 0.5–2.0 MeV/nuc $^3\text{He}/^4\text{He}$ between 2 and 194 times the average SSW ratio. Two competing ideas have been suggested: 1) reacceleration of remnant flare suprathermal ions by CME-driven shocks in corona and interplanetary (IP) space (e.g., Mason et al. 1999) and 2) simultaneous flare (jet)-related acceleration in parent active regions (ARs) or other sites in the corona (e.g., Cane et al. 2003).

2. Results

2.1. Event selection

We browsed Hart et al. (2022) catalog of ^3He -rich periods, covering 1997 Sep 29 – 2021 Mar 1, for coincidences with GSEP events measured by SOHO ERNE (Torsti et al. 1995). During the SDO era (after May 2010), our interval of interest, 174 ACE ULEIS (Mason et al. 1998) ^3He -rich periods were reported in the catalog. We selected proton events that are sufficiently intense at high energies. Specifically, we require that the ratio between 25–50 MeV proton intensity peak and 24-hr background before the event onset is greater than two. In addition to ^3He periods that occurred during GSEP events (i.e., coincidences), we found cases when ^3He periods closely ended before the events. Since these periods would contain suprathermal seed particles for further re-acceleration by CME-driven shocks, we included them in this study. Namely, we adopted ^3He periods ending within one day before proton event onset. We note

Table 1. 25–50 MeV proton event characteristics

| # | # | Proton event start day | GOES X-ray flare | | CME | | Jet | ${}^3\text{He}/{}^4\text{He}$ ($\times 10^2$) | Ref. |
|----|-----|---------------------------|------------------|-------|-------|-------|-----|---|------------|
| | | | Start | Class | Speed | Width | | | |
| 1 | 470 | 2010-Jun-12 ^b | 00:54:00 | M2.0 | 486 | 119 | N | 1.54±0.18 | i, j, k, l |
| 2 | 473 | 2010-Aug-31 ^{ab} | ... | ... | 1304 | 360 | Y | 0.68±0.39 | i, k, l |
| 3 | 494 | 2011-Jan-28 ^b | 00:44:00 | M1.3 | 606 | 119 | Y | 4.08±0.93 | i |
| 4 | 508 | 2011-Apr-21 ^{ab} | ... | ... | 475 | 111 | Y | 43.57±19.83 | i |
| 5 | 524 | 2011-Aug-02 ^b | 05:19:00 | M1.4 | 712 | 268 | N | ... | i |
| 6 | 525 | 2011-Aug-08 | 18:00:00 | M3.5 | 1343 | 237 | N | 1.05±0.09 | i |
| 7 | 539 | 2011-Nov-26 ^b | 06:09:00 | C1.2 | 933 | 360 | N | 0.32±0.03 | i, m |
| 8 | 554 | 2012-Jan-19 ^b | 13:44:00 | M3.2 | 1120 | 360 | N | 0.99±0.08 | i |
| 9 | 566 | 2012-May-17 ^b | 01:25:00 | M5.1 | 1582 | 360 | N | 0.35±0.04 | i, m |
| 10 | 571 | 2012-Jun-14 ^b | 12:52:00 | M1.9 | 987 | 360 | N | 0.29±0.06 | i |
| 11 | 604 | 2013-Feb-26 ^{ab} | ... | ... | 987 | 360 | N | 0.59±0.19 | i |
| 12 | 611 | 2013-May-02 | 04:58:00 | M1.1 | 671 | 99 | Y | 20.05±2.57 | i, j, n |
| 13 | 641 | 2013-Sep-30 ^b | 21:43:00 | C1.2 | 1179 | 360 | N | 0.36±0.04 | i, j |
| 14 | 647 | 2013-Oct-25 ^b | 07:53:00 | X1.7 | 587 | 360 | Y | 2.45±0.33 | i |
| | | | 14:51:00 | X2.1 | 1081 | 360 | N | | i |
| 15 | 665 | 2013-Dec-26 ^{ab} | ... | ... | 1011 | >171 | N | 2.28±0.56 | i |
| 16 | 668 | 2014-Jan-04 | 18:47:00 | M4.0 | 977 | 360 | Y | 0.29±0.08 | m |
| 17 | 682 | 2014-Feb-25 ^b | 00:39:00 | X4.9 | 2147 | 360 | N | 0.30±0.03 | |
| 18 | 692 | 2014-Apr-18 | 12:31:00 | M7.3 | 1202 | 360 | Y | 0.69±0.06 | j |
| 19 | 700 | 2014-May-07 | 16:07:00 | M1.2 | 923 | 360 | Y | 1.96±0.57 | |
| 20 | 715 | 2014-Jun-12 | 21:34:00 | M3.1 | 684 | 186 | Y | 4.20±0.30 | |
| 21 | 781 | 2015-Jul-19 | 09:22:00 | C2.1 | 782 | 194 | N | 0.35±0.27 | |
| 22 | 789 | 2015-Sep-20 | 17:32:00 | M2.1 | 1239 | 360 | N | 0.49±0.07 | |
| 23 | 790 | 2015-Sep-30 | 16:54:00 | C2.4 | ... | ... | Y | 0.58±0.06 | j |

Notes. ^aEvents with backside source. ^bEvents measured at least on one of the two STEREO spacecraft.

References. (i) Richardson et al. (2014), (j) Cliver et al. (2019), (k) Wiedenbeck et al. (2013), (l) Bučík et al. (2016), (m) Desai et al. (2016), (n) Nitta et al. (2015)

we did not find in the catalog a ${}^3\text{He}$ -period ending within two days before proton event onset. 41 coincidences fulfill the above criteria. Ten events at low (<1 MeV/nuc) ULEIS energies did not show ${}^4\text{He}$ (and often O) intensity increase above the previous background and were not included. Furthermore, seven ion enhancements were measured during corotating interaction regions (CIRs) and one during an IP shock. These events were also excluded. The CIRs were identified based on typical solar wind plasma and IP magnetic field behavior. The IP shock is reported in the database by Oliveira (2023). Thus, we have 23 events left to explore.

Table 1 shows the solar characteristics of proton events. Column 1 marks the event number. Column 2 shows the corresponding ${}^3\text{He}$ -rich period number (Hart et al. 2022). Column 3 indicates the start day of the proton event at 25–50 MeV. Columns 4 and 5 show GOES X-ray start time (with day in column 3) and class as obtained from the NOAA Space Weather Prediction Center (SWPC) Edited Events list. Events #2, 4, 11, and 15 have a backside source. A flare for event #13 started on an earlier day than the proton event start day. Note that event #14 was associated with multiple flares. Columns 6 and 7 indicate CME speed (km/s) and width ($^\circ$) from the LASCO manually identified CME catalog[†] (Yashiro et al. 2004). Event #23 has not reported CME. Column 8 indicates with Y a jet in the parent AR as observed by SDO AIA (Lemen et al. 2012) or STEREO EUVI (Howard et al. 2008). Column 9 shows 0.5–2.0 MeV/nuc ${}^3\text{He}/{}^4\text{He}$. Note that independent ISEP events that occurred during some proton events were excluded from the ${}^3\text{He}/{}^4\text{He}$ calculation (details in Section 2.2). The last column marks references to earlier studies of these events. All events except #21 and #23 were associated with type II radio bursts. The radio bursts were reported in the SWPC list or identified using STEREO-A, -B (Bougeret et al. 2008), or Wind (Bougeret et al. 1995) radio spectrograms. 14 events were measured at least on one of the two STEREO spacecraft by HET (von Rosenvinge et al. 2008) at the proton energy range 24–41 MeV. The minimum longitudinal

[†] https://cdaw.gsfc.nasa.gov/CME_list/

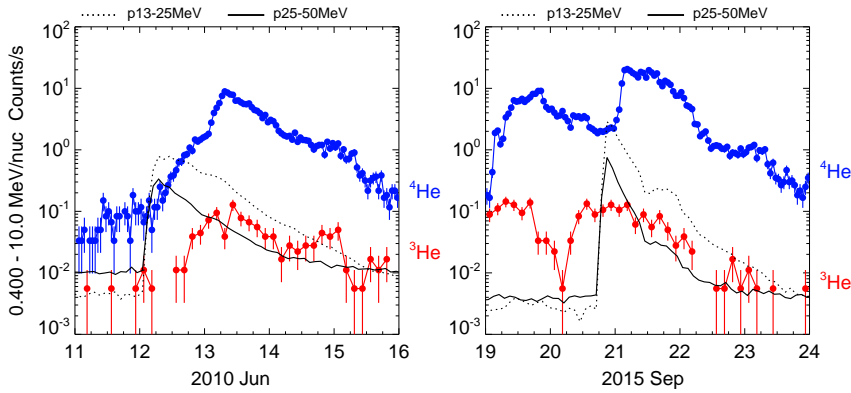


Figure 1. ACE ULEIS 3-hr ^3He (2.8–3.1 AMU) and 1-hr ^4He (3.5–6.0 AMU) count rates in events #1 (left) and #22 (right). Overplotted are SOHO ERNE proton fluxes (in arbitrary units) in two energy ranges.

separation between Earth and STEREO was 70° , implying that these events were widespread. Five events (#7, 9, 13, 17, and 18) are on the NOAA list of Solar Proton Events Affecting the Earth’s Environment \ddagger .

2.2. Observations

It has been argued that similar time profiles of ^3He with other ion species suggest the common acceleration and transport origin (Mason et al. 1999; Wiedenbeck et al. 2000). Four events (#15, 18, 21, 22) show distinct time profiles of ^3He and ^4He , caused by ^3He left over from preceding impulsive (^3He -rich) events. Six events (#1, 3, 4, 5, 9, 14) from the remaining 19 events contain independent ^3He -rich SEP enhancement, which also leads to distinct time profiles. The periods of independent ^3He enhancements were excluded from four events (#1, 5, 9, 14) by adjusting the integration interval. It was not possible in two events (#3, 4) where the independent ^3He -rich period spanned nearly the whole proton event. Thus, we have 17 events to explore. Figure 1 (left) shows event #1 (included in the final list) with preceding ^3He ions, similar time profiles of ^3He and ^4He during proton flux decay until the beginning of 2010 Jun 14. Later, the increase in ^3He count rates is due to an independent ISEP event accompanied by solar energetic electrons detected by ACE EPAM (Gold et al. 1998). Figure 1 (right) shows event #22 (excluded from the final list) with ^3He left over from the preceding ISEP event. During a sudden rise in ^4He count rates on 2015 Sep 21, associated with the GSEP event, ^3He count rates continued to decrease.

The $^3\text{He}/^4\text{He}$ ratio was determined using helium (2–5 AMU) mass histograms. The ratio is calculated in the broad energy range of 0.5–2.0 MeV/nuc, ensuring enough ^3He counts. We fitted the background at 2.00–2.64 AMU and spillover from ^4He at 3.28–3.52 AMU with two $\log(y) = a + bx$ functions, where a and b are parameters, and x corresponds to mass and y to ion counts. Both fits were extrapolated to the ^3He range (2.8–3.2 AMU), and the number of counts under the fit was subtracted from the total number of ^3He counts. Net ^4He counts were obtained from the 3.5–5.0 AMU range. Figure 2 shows event #08, where background and spillover were removed, and event #19, with no background and spillover. After adjusting integration intervals to eliminate independent ^3He events, the ^3He counts in #5 dropped to zero. In the remaining events, the ^3He peaks are finite - the number of net ^3He counts is 2σ or more above zero (same as in Desai et al. 2006).

\ddagger <https://umbra.nascom.nasa.gov/SEP/>

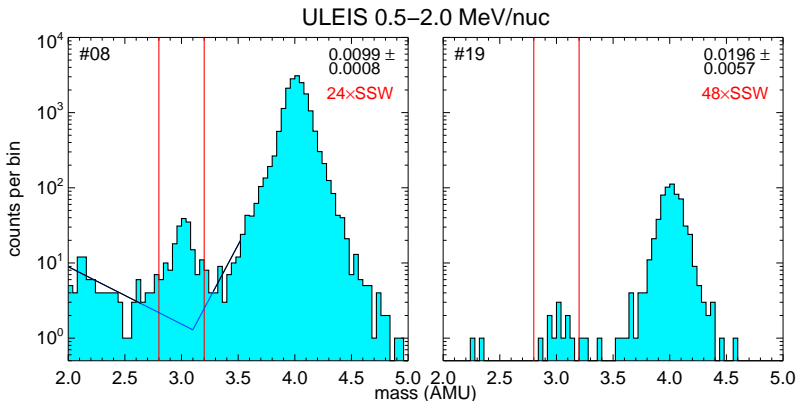


Figure 2. He mass histograms for events #8 (left) and #19 (right). The vertical red lines mark the ^3He mass range. The $^3\text{He}/^4\text{He}$ ratios are shown in the upper right corner. Left: The two tilted lines are the least square fits of the background and ^4He spillover (black) and the extrapolations to the ^3He range (blue).

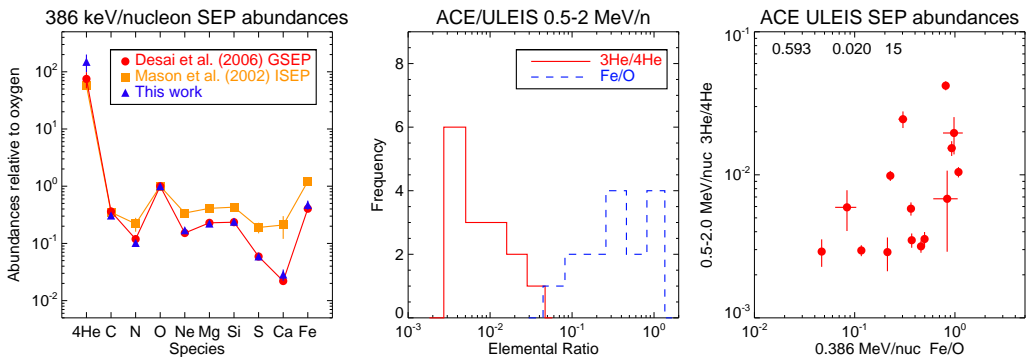


Figure 3. Left: Survey-averaged abundances relative to O in this work (blue triangles), GSEP (red circles), and ISEP (orange squares) reference abundances. Middle: Distribution of 0.5–2.0 MeV/nuc $^3\text{He}/^4\text{He}$ (red solid line) and 386 keV/nuc Fe/O (blue dashed line). Right: $^3\text{He}/^4\text{He}$ vs. Fe/O. The three numbers indicate the Spearman correlation coefficient, p -value, and sample size.

Figure 3 (left) displays the survey-averaged abundances using 16 events in Table 1 (#1, 2, 5–11, 13, 14, 16, 17, 19, 20, 23). Event #12 was not included in the averaging. This event was on the ISEP event list by Nitta et al. (2015). Indeed, the event 0.5–2.0 MeV/nuc $^3\text{He}/^4\text{He} = 0.20 \pm 0.03$ ($492 \times \text{SSW}$ value) is exceptionally high. Furthermore, the abundances of Si, S, and Fe are ISEP-like, and Ne and Mg are enhanced compared to GSEP values. Figure 3 (left) shows that the relative abundances in this work are consistent with reference GSEP abundances. Table 2 lists the average heavy-ion abundances of this survey along with GSEP (Desai et al. 2006) and ISEP (Mason et al. 2002) average abundances. Figure 3 (middle) indicates that $^3\text{He}/^4\text{He}$ peaks at the lowest values while Fe/O shows a more uniform distribution. Some high Fe/O can be due to rigidity-dependent transport effects. This will be explored in the next study. Minimum, maximum, mean, and median $^3\text{He}/^4\text{He}$ expressed as multipliers of the SSW value ($4.08 \pm 0.25 \times 10^{-4}$) are 7, 103, 26 ± 7 , and 15, respectively. Figure 3 (right) shows a moderate positive correlation ($r = 0.593$) between $^3\text{He}/^4\text{He}$ and Fe/O with a low probability of 2% that ratios are a random sample. Note that because ^3He dropped to zero in #5, both the middle and right panels involve 15 events. Desai et al. (2006) reported $r = 0.66$ (for 29 events with a finite ^3He peak), but after excluding two outliers, r dropped to 0.026. The authors concluded that Fe/O is independent of $^3\text{He}/^4\text{He}$ in GSEP events. Similar observations have been reported in ISEP events (Mason et al. 1986; Reames et al. 1994).

Table 2. Average heavy ion abundances

| Element | GSEP ^a (386 keV/nuc) | GSEP ^b (385 keV/nuc) | ISEP ^c (385 keV/nuc) |
|---------------------------|------------------------------------|------------------------------------|------------------------------------|
| ^4He | 149.5 ± 50.7 | 75.0 ± 23.6 | 57 ± 7.79 |
| C | 0.308 ± 0.014 | 0.361 ± 0.012 | 0.35 ± 0.08 |
| N | 0.102 ± 0.004 | 0.119 ± 0.003 | 0.22 ± 0.06 |
| O | $\equiv 1.0 \pm 0.02$ | $\equiv 1.0 \pm 0.02$ | $\equiv 1.0 \pm 0.14$ |
| Ne | 0.170 ± 0.015 | 0.152 ± 0.005 | 0.34 ± 0.06 |
| Mg | 0.223 ± 0.018 | 0.229 ± 0.007 | 0.41 ± 0.07 |
| Si | 0.240 ± 0.022 | 0.235 ± 0.011 | 0.43 ± 0.06 |
| S | 0.059 ± 0.005 | 0.059 ± 0.004 | 0.19 ± 0.04 |
| Ca | 0.029 ± 0.006 | 0.022 ± 0.002 | 0.21 ± 0.09 |
| Fe | 0.472 ± 0.087 | 0.404 ± 0.047 | 1.21 ± 0.14 |
| Ratio | (0.5–2.0 MeV/nuc) | (0.5–2.0 MeV/nuc) | (385 keV/nuc) |
| $^3\text{He}/^4\text{He}$ | 0.011 ± 0.003 | 0.006 ± 0.002 | 0.354 ± 0.137 |

Notes. ^aThis work. ^bFrom Desai et al. (2006). ^cFrom Mason et al. (2002).

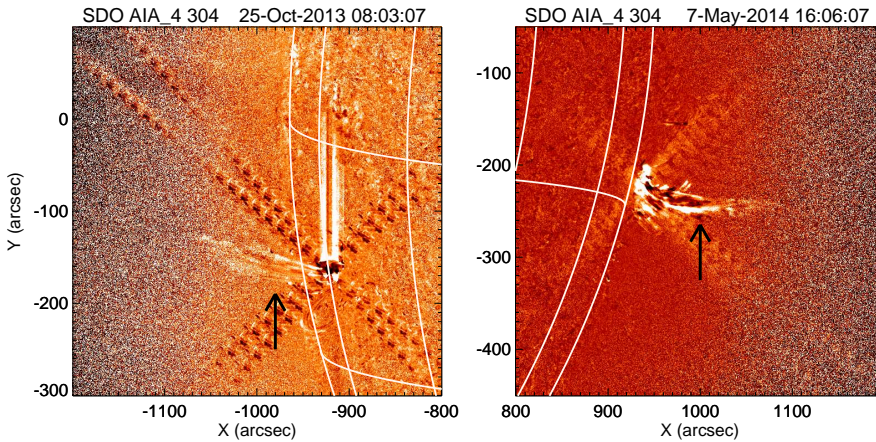


Figure 4. 1-min running difference SDO AIA 304 Å images of source flares in events #14 (Left panel; X1.7 flare at E75) and #19 (Right panel; M1.2 flare at W90). Jet expulsions are marked by arrows. Vertical bright stripes in the left panel are saturation, and diagonal patterns in both panels are diffraction fringes due to a strong EUV signal.

Figure 4 shows the source flare for two events. Along with the bright flares that left some artifacts in the EUV images, ejections of jets from the sources were observed. Jets, a signature of magnetic reconnection involving field lines open to IP space, have been associated with the source of ^3He -rich SEPs (e.g., Bučík 2020; Nitta et al. 2023, and references therein).

Note that events #1 and #2 were included in the list of ISEP events by Wiedenbeck et al. (2013) and Bučík et al. (2016). The events had $^3\text{He}/^4\text{He}$ of $38 \times \text{SSW}$ and $17 \times \text{SSW}$ ratios, respectively. These values are typical for ^3He -enriched GSEP events. The heavy ions showed mixed composition (N, S with GSEP and Ne, Fe with ISEP abundances) in event #1 and GSEP composition (except Fe) in event #2. In addition, these events were widespread and associated with type II radio bursts.

3. Conclusion

We explored the ^3He origin in 23 high-energy (25–50 MeV) proton events. Except for independent ISEP events starting just before or during proton events, the ^3He origin in 15 events has no simple cause (presumed ISEP event #12 is not counted). 14 out of 15 events in this study showed preceding remnant ^3He . All these 14 events showed similar ^3He & ^4He intensity-time profiles, suggesting that reacceleration of remnant material by the associated CME shock

was the most probable cause of ^3He enhancement. The origin of ^3He ions in one event (#10) remains unclear. In 6 events (those with preceding remnant ^3He ions), there were observed simultaneous jets in parent ARs. Interestingly, three events (#19, 14, 20) with the highest $^3\text{He}/^4\text{He}$ were associated with jets. This signifies the role of jets as a simultaneous source of energetic ^3He in GSEP events.

R.B. acknowledges support by NASA grants 80NSSC21K1316 and 80NSSC22K0757. The LASCO C2 CME catalog is generated and maintained at the CDAW Data Center by NASA and The Catholic University of America in cooperation with the Naval Research Laboratory. SOHO is a project of international cooperation between ESA and NASA.

References

- Bougeret, J. L., Goetz, K., Kaiser, M. L., *et al.* 2008, *Space Sci. Revs*, 136(1-4), 487–528.
- Bougeret, J. L., Kaiser, M. L., Kellogg, P. J., *et al.* 1995, *Space Sci. Revs*, 71(1-4), 231–263.
- Bučík, R. 2020, *Space Sci. Revs*, 216(2), 24.
- Bučík, R., Innes, D. E., Mason, G. M., & Wiedenbeck, M. E. 2016, *ApJ*, 833(1), 63.
- Cane, H. V., von Roseninge, T. T., Cohen, C. M. S., & Mewaldt, R. A. 2003, *Geophys. Res. Lett.*, 30(12), 8017.
- Cliver, E. W., Kahler, S. W., Kazachenko, M., & Shimojo, M. 2019, *ApJ*, 877(1), 11.
- Desai, M. I., Mason, G. M., Dayeh, M. A., *et al.* 2016, *ApJ*, 816(2), 68.
- Desai, M. I., Mason, G. M., Gold, R. E., *et al.* 2006, *ApJ*, 649(1), 470–489.
- Gloeckler, G. & Geiss, J. 1998, *Space Sci. Revs*, 84, 275–284.
- Gold, R. E., Krimigis, S. M., Hawkins, S. E., I., *et al.* 1998, *Space Sci. Revs*, 86, 541–562.
- Hart, S. T., Dayeh, M. A., Bučík, R., *et al.* 2022, *ApJS*, 263(2), 22.
- Howard, R. A., Moses, J. D., Vourlidas, A., *et al.* 2008, *Space Sci. Revs*, 136(1-4), 67–115.
- Lemen, J. R., Title, A. M., Akin, D. J., *et al.* 2012, *Solar Phys.*, 275(1-2), 17–40.
- Mason, G. M., Gold, R. E., Krimigis, S. M., *et al.* 1998, *Space Sci. Revs*, 86, 409–448.
- Mason, G. M., Mazur, J. E., & Dwyer, J. R. 1999, *ApJ Letters*, 525(2), L133–L136.
- Mason, G. M., Reames, D. V., Klecker, B., *et al.* 1986, *ApJ*, 303, 849.
- Mason, G. M., Wiedenbeck, M. E., Miller, J. A., *et al.* 2002, *ApJ*, 574(2), 1039–1058.
- Nitta, N. V., Bučík, R., Mason, G. M., *et al.* 2023, *Front. Astron. Space Sci.*, 10, 50.
- Nitta, N. V., Mason, G. M., Wang, L., *et al.* 2015, *ApJ*, 806(2), 235.
- Oliveira, D. M. 2023, *Front. Astron. Space Sci.*, 10, 1240323.
- Reames, D. V., Meyer, J. P., & von Roseninge, T. T. 1994, *ApJS*, 90, 649.
- Richardson, I. G., von Roseninge, T. T., Cane, H. V., *et al.* 2014, *Solar Phys.*, 289(8), 3059–3107.
- Torsti, J., Valtonen, E., Lumme, M., *et al.* 1995, *Solar Phys.*, 162(1-2), 505–531.
- von Roseninge, T. T., Reames, D. V., Baker, R., *et al.* 2008, *Space Sci. Revs*, 136(1-4), 391–435.
- Wiedenbeck, M. E., Christian, E. R., Cohen, C. M. S., *et al.* In Mewaldt, R. A., Jokipii, J. R., Lee, M. A., Möbius, E., & Zurbuchen, T. H., editors, *Acceleration and Transport of Energetic Particles Observed in the Heliosphere 2000*, volume 528 of *American Institute of Physics Conference Series*, pp. 107–110.
- Wiedenbeck, M. E., Mason, G. M., Cohen, C. M. S., *et al.* 2013, *ApJ*, 762(1), 54.
- Yashiro, S., Gopalswamy, N., Michalek, G., *et al.* 2004, *J. Geophys. Res. Space Phys.*, 109(A7), A07105.